

## Photomultiplier tubes in the MiniBooNE experiment

S.J. Brice<sup>a</sup>, L. Bugel<sup>b</sup>, J.M. Conrad<sup>b</sup>, B. Fleming<sup>c</sup>, L. Gladstone<sup>b,\*</sup>, E. Hawker<sup>d</sup>, P. Killewald<sup>e</sup>,  
J. May<sup>f</sup>, S. McKenney<sup>g</sup>, P. Nienaber<sup>h</sup>, B. Roe<sup>e</sup>, V. Sandberg<sup>g</sup>, D. Smith<sup>i</sup>, M. Wysocki<sup>e</sup>

<sup>a</sup>Fermi National Accelerator Laboratory, Batavia IL 60510, USA

<sup>b</sup>Columbia University, Pupin Laboratories, 538 W. 120th St., New York NY 10027, USA

<sup>c</sup>Yale University, New Haven CT 06520, USA

<sup>d</sup>Western Illinois University, Currens Hall, Macomb IL 61455, USA

<sup>e</sup>University of Michigan, Department of Physics, Ann Arbor MI 48109, USA

<sup>f</sup>Stanford Linear Accelerator Center, Menlo Park CA 94025, USA

<sup>g</sup>Los Alamos National Laboratory, Los Alamos NM 87545, USA

<sup>h</sup>Saint Mary's University of Minnesota, Winona MN 55987, USA

<sup>i</sup>Embry-Riddle Aeronautical University, Prescott AZ 86301, USA

Received 9 February 2006; accepted 15 February 2006

Available online 20 March 2006

### Abstract

The detector for the MiniBooNE [Proposal for the MiniBooNE experiment: (<http://www-boone.fnal.gov/publicpages/proposal.ps>)] experiment at the Fermi National Accelerator Laboratory employs 1520 8 in. Hamamatsu models R1408 and R5912 photomultiplier tubes with custom-designed bases. Tests were performed to determine the dark rate, charge and timing resolutions, double-pulsing rate, and desired operating voltage for each tube, so that the tubes could be sorted for optimal placement in the detector. Seven phototubes were tested to find the angular dependence of their response. After the Super-K phototube implosion accident, an analysis was performed to determine the risk of a similar accident with MiniBooNE.

© 2006 Elsevier B.V. All rights reserved.

PACS: 29.40.Ka

Keywords: MiniBooNE; Phototube; Photomultiplier tube; R1408; R5912

### 1. Introduction

The MiniBooNE experiment [1] is a  $\nu_\mu \rightarrow \nu_e$  oscillation search at Fermi National Accelerator Laboratory designed to confirm or rule out the LSND signal [2]. The Fermilab Booster accelerates protons to 8 GeV; these protons strike a beryllium target, generating mesons which decay to produce the MiniBooNE  $\nu_\mu$  beam. The neutrinos interact in a 12 m diameter sphere filled with mineral oil of food-grade purity, and the Cherenkov light from charged particles produced in these interactions is detected by 8 in. Hamamatsu [3] photomultiplier tubes (PMTs) lining the sphere. There are 1280 PMTs in the light-tight inner signal region: 956 are Hamamatsu model R1408, inherited

from the LSND experiment; the remainder are Hamamatsu model R5912. Light produced in the outer concentric veto region is detected by an additional 240 R5912 PMTs. A typical tube is pictured in Fig. 1. Light signatures recorded by the PMTs are used to reconstruct events within the detector. Leptons from charged current neutrino interactions are of particular interest, since these leptons tag the incoming neutrino flavor.

It is important to sufficiently understand the operating characteristics of the PMTs, since they are the only active detector element in MiniBooNE. MiniBooNE uses a Monte Carlo simulation to understand the detector's response to neutrino interactions. This program simulates photons traveling through the detector from creation to detection, and models all intermediate processes. The geometry of all detector elements is coded into the simulation, including that of the PMTs.

\*Corresponding author. Tel.: +1 917 647 5099; fax: +1 212 854 3379.  
E-mail address: [leg2102@columbia.edu](mailto:leg2102@columbia.edu) (L. Gladstone).



Fig. 1. A typical phototube used in the MiniBooNE detector: an 8 in. R1408 mounted on its wire frame. The base is coated with Masterbond (as described in Section 2.1) before the PMT is installed into the detector.

Photons striking the photocathode in a PMT produce photoelectrons (PEs), whose number is amplified via a dynode chain; the magnitude of the current so produced is proportional to the number of incident photons whose energy is above a certain threshold. A specific operating voltage must be found for each PMT so that all tubes have the proper gain. Gain is defined here as observed output charge (divided by charge per electron) per input photoelectron. The charge and timing information recorded from each PMT can then be used to reconstruct the events off-line. Ideally, this information, along with photocathode efficiency as determined by Hamamatsu, specifies exactly when and how many photons hit the PMT. Each PMT is tested in several ways to determine: basic functionality, timing resolution, charge resolution, dark rate and operating voltage. The operating voltage was chosen so that the gain is closest to the desired  $1.6 \times 10^7$  signal electrons per photoelectron.

In addition to these global PMT tests, specialty tests were done on seven PMTs. In order for the Monte Carlo simulation to properly model the behavior of the PMTs, it is necessary to correctly include their efficiency as a function of incident photon angle. The dominant effect comes simply from the solid angle subtended by a PMT as a function of angle, and this is handled by coding an approximate PMT shape into the simulation. Any remaining efficiency function must be measured and entered into the code. The measurement, however, will itself contain the solid angle effects; these must be factored out of the measured angular efficiency to avoid double-counting. A thorough understanding of the angle-dependent response, time and charge resolution, and individual variations of the

photomultiplier tubes will help accurately identify neutrino events within the MiniBooNE detector.

This paper discusses the following topics. In Section 2, the technical specifications of the phototubes are described, along with the custom bases that MiniBooNE used. In Section 3, the tests which were performed on every tube, with their results, are described. In Section 4, the angular tests which were performed on seven tubes are described, along with their results and a comparison of these results to other angular tests. Section 5 describes the studies of MiniBooNE's risk of an implosion chain reaction.

## 2. Technical design of the PMTs

Phototubes in the MiniBooNE detector satisfy the following technical requirements. Their maximum dark rates lie below the response rate expected from cosmic rays. Their gains are high, around  $10^7$ , to be adequately sensitive. Their responses are reliably fast, and have a narrow enough pulse width to minimize response pileup. Each of these characteristics was tested; these tests are described in subsequent sections.

### 2.1. PMT specifications from Hamamatsu and custom base design

The two models (R5912 and R1408) of phototubes used in MiniBooNE differ primarily in their dynode structures and number of stages, and are similar in all the characteristics described above.

The R5912 is a 10-dynode-stage photomultiplier tube with an 8 in. hemispherical photocathode. The base supplies the high voltages for the grids, dynodes, and anode, and provides the back termination in the anode circuit. The voltage divider chain is entirely passive, and is fabricated with carbon-film resistors and ceramic-disk capacitors. A single coaxial cable is used to provide high voltage (on the order of 1500 V) and to connect the anode signal to the readout. The anode circuit is back terminated in  $50\Omega$  and balanced to compensate for the distortion caused by the capacitive coupling in the termination circuit. The high voltage taper is the one recommended by Hamamatsu (ca. 1996) for gain. A drawing of the tube dome and a diagram of the dynode circuitry from the Hamamatsu data sheets are included in the appendix as Fig. A.1. Fig. 2 shows the printed circuitboard layout for the R5912 custom bases.

The R1408 is a nine-dynode-stage photomultiplier tube. Hamamatsu upgraded it to the R5912 at least 10 years before this publication. The circuit diagram for the base (designed for the LSND experiment) is shown in Fig. 3.

The detector design requires that the tubes, bases, and cables be immersed in oil for several years without adversely affecting the phototubes or the oil. To accomplish this, the bases and necks of all MiniBooNE PMTs were coated with the two-component epoxy EP21LV from Masterbond [4], which is impervious to and insoluble in oil.

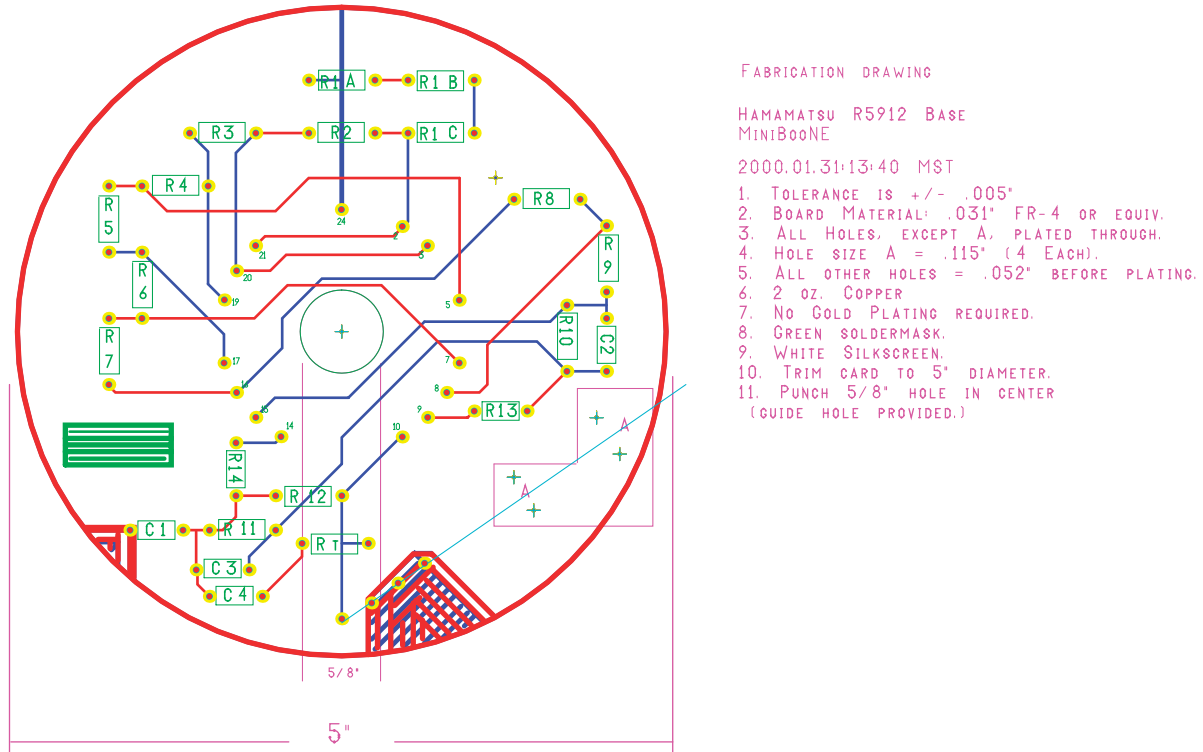


Fig. 2. The printed circuit artwork and layout for the custom bases of the R5912 phototubes. The design is a two-sided card made from epoxy fiberglass (G10). For a circuit schematic, see Fig. A.1.

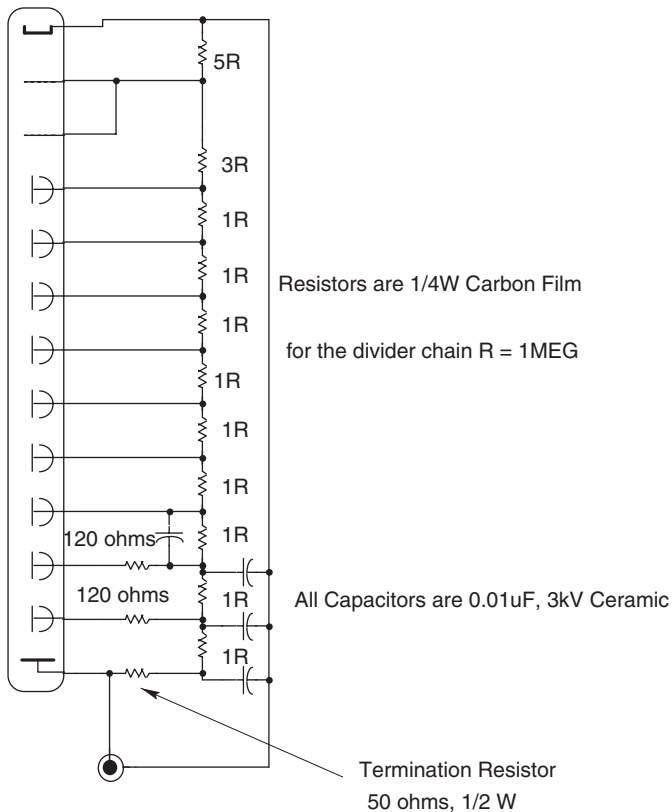


Fig. 3. Schematic diagram of the base used for the R1408 photomultiplier tube.

For the R1408 tubes recycled from LSND, the Masterbond was applied on top of the existing Hysol [5] coating.

### 3. Global testing

The method of global testing for the PMTs has been described in detail elsewhere [6]; a synopsis of that report is provided here.

The purpose of global testing was to select an operating voltage which resulted in a similar response from each PMT, regardless of model (R1408 or R5912). The selected gain was  $1.6 \times 10^7$  electrons per photoelectron (PE).

The testing process served to determine five characteristic data about each PMT: dark rate, time jitter, charge resolution, double-pulsing rate, and pulse shape. These data were used to sort the tubes into five categories, from best to worst in timing and charge resolution. Categories 4 and 5 had similar resolutions, and were divided between the two categories by dark rate. These classifications were used to distribute tubes ranked 1 through 4 (with about 320 in each rank) evenly throughout the tank. Category 5 tubes were used in the veto, where timing and charge resolution is less crucial but low dark rate is important.

#### 3.1. Global testing: apparatus

Fig. 4 shows a schematic of a single tube in the test setup. The full setup accommodated 30 R1408 PMTs and 16

R5912 PMTs. Tubes were dark adapted for 12–24 h. After this, tube responses were recorded using an automated VXI readout system. Fiber optic cables located about eight inches from the face of each tube transmitted a steady stream of pulses from an LED pulser. A diagram of a signal tube setup is shown in Fig. 4.

The output pulse was sent to the VXI electronics, where the waveform was digitized (Fig. 5). Different delays were added to the LED trigger to center the captured waveform in the time windows (Fig. 6). The pulses were digitized over 512 channels at a rate of 5 giga-samples/s using the Tektronix oscilloscope inside the VXI crate.

### 3.2. Global testing: procedures and data handling

The testing data were acquired in two modes. First, the dark rate rates were collected by recording the noise rates measured at a range of operating voltages, with no light source. Second, the PMTs were illuminated by an LED light source whose wavelength was 450 nm (corresponding approximately to the Cherenkov frequency of the oil). The source flashed at a rate of 1 kHz; the width of each pulse was 1 ns. PMT responses to 600–1000 LED flashes were used to determine the operating voltage for the required gain. This procedure also allowed both the charge and time resolutions, and pre- and post-pulsing anomalies to be studied.

### 3.3. Global testing: results

Each PMT was tested to determine its operating voltage, as well as its gain, dark rate, charge resolution, timing resolution, and double pulsing rate. The results of the later five measurements are reported below.

PMT gain corresponds to the mean number of electrons produced by the phototube in response to one PE. This was determined using the equation

$$\text{gain} = \left( \frac{Q_{\text{tot}}}{N} \right) \left( \frac{1 - e^{-\mu}}{\mu} \right),$$

where  $Q_{\text{tot}}$  is the total charge from the PMT for all pulses with response past threshold,  $N$  is the number of responses past threshold, and  $\mu$  is the light level. Total charge was computed by summing up charge in the main PMT pulse for all responses with in-time pulses that pass threshold, excluding double pulses. The second factor is the reciprocal

of the average number of PEs seen by a PMT for a given light level,  $\mu$ , (excluding zero responses) predicted from Poisson statistics. The voltage was selected in order to obtain a gain of  $1.6 \times 10^7$  electrons per PE. The distribution of operating voltages at which the PMTs run in the detector is shown in Fig. 7.

Dark rate is defined as the number of pulses larger than 3 mV in 1 s. The experiment required that the tubes operate with a dark rate below 8 kHz in the main tank and below 4 kHz in the veto. Dark rates were measured over a range of voltages, from several hundred volts below suggested operating voltage up to operating voltage and above. Plots of dark rate versus voltage, or plateau plots, serve as a measure of PMT quality. The PMTs are operated on the plateau, where dark rate does not change significantly as the operating voltage increases. The R1408 PMTs were found to have poorly defined plateaus, but they were considered acceptable if the dark rates had a steady, shallow rise when the operating voltage was increased.

The charge resolution,  $\sigma_q$  is determined from the width of the peak in the PMT response corresponding to one PE. The distribution of charge resolutions for all PMTs is shown in Fig. 8.

The time jitter in the measurements is dominated by the timing resolution of the PMTs; the timing resolution of the oscilloscope was found to be negligible. The distribution of timing resolutions for all PMTs is shown in Fig. 9.

Pre- and post-pulsing, where the main PMT pulse is preceded or followed by additional small pulses, is a known effect in the types of PMTs used on MiniBooNE [6]. Pre-pulsing was observed in only four R1408 tubes, which were rejected. Post-pulsing occurs in two different time intervals: between 8 and 60 ns after the main pulse, and 100 ns–16  $\mu$ s after the main pulse. MiniBooNE is concerned about the first case (“early post-pulsing”), because data in the detector are recorded in 100 ns intervals, making it unlikely that the second case will contaminate events. Early post-pulsing can begin when an electron accelerated to the first dynode starts a typical cascade, and causes another electron to be ejected from the first dynode. This second electron can move around the inside of the PMT dome before settling back to the first dynode and initiating a second cascade, which becomes the post-pulse. Hamamatsu reports that R5912 and R1408 PMTs are expected to have early post-pulses in 3% of the responses from every tube. MiniBooNE observed higher rates. PMTs

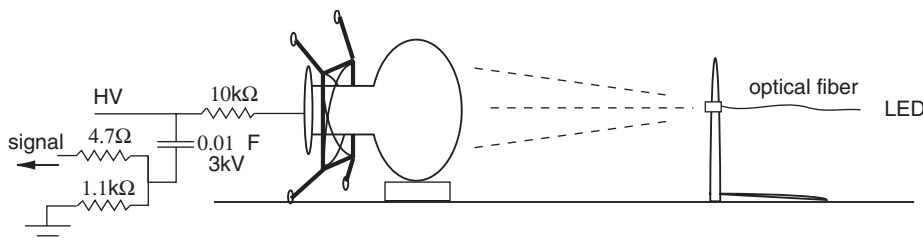


Fig. 4. The test setup used to measure the response of PMTs at low light levels (not to scale). The pulse is picked off the high voltage line shown in the left side of the figure.

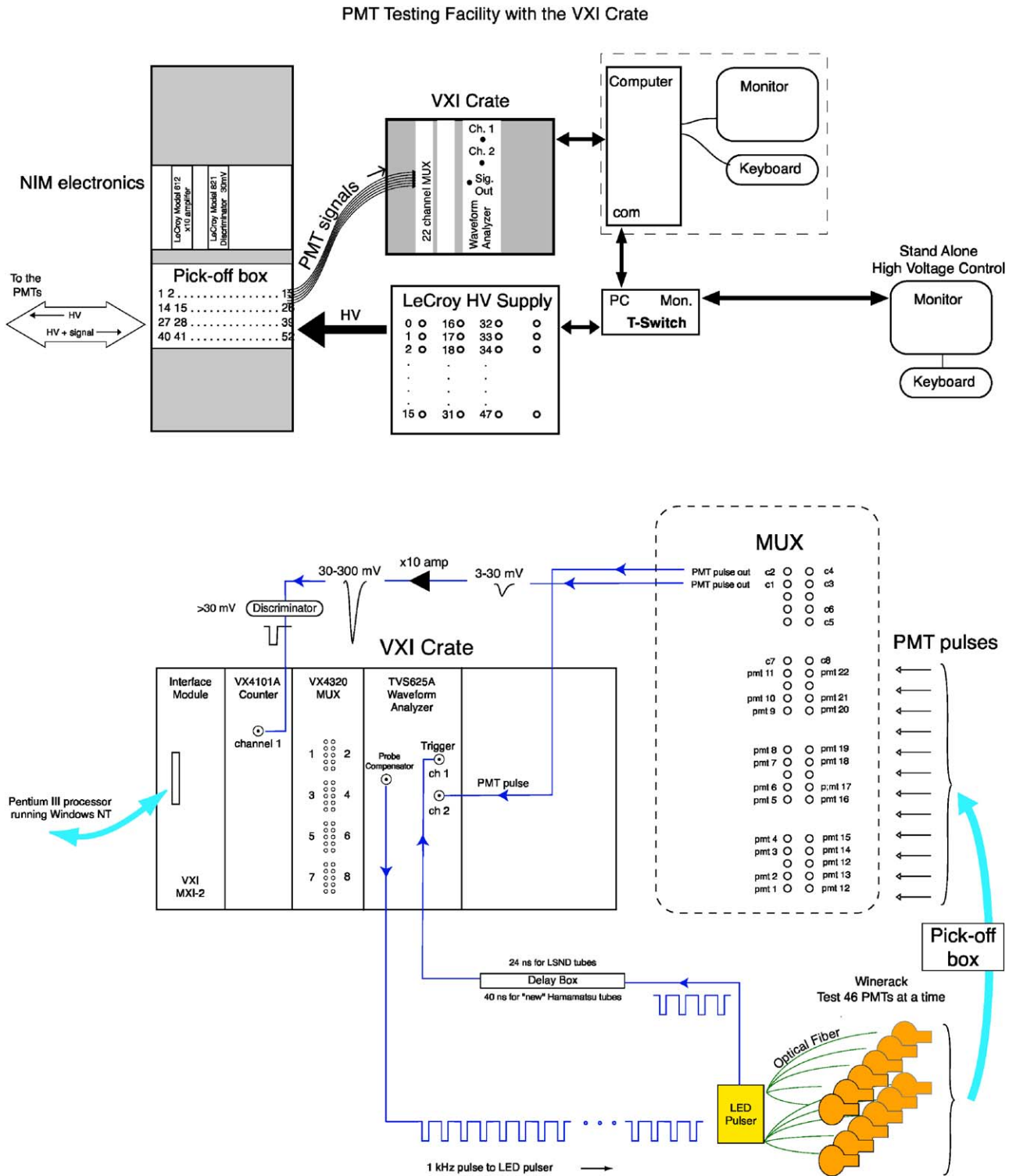


Fig. 5. A schematic of the PMT testing facility data acquisition system. The PMT responses to an LED pulser are acquired from the HV input and analyzed in the VXI crate (from Ref. [6]).

were required to have a double-pulsing rate of <6% for the R5912 PMTs and 3% for the R1408 PMTs at the time of installation. The distribution of PMT double-pulsing rates for all PMTs is shown in Fig. 10.

#### 4. Angular testing

Extensive specialized testing was done on seven phototubes to explore the behavior of other important

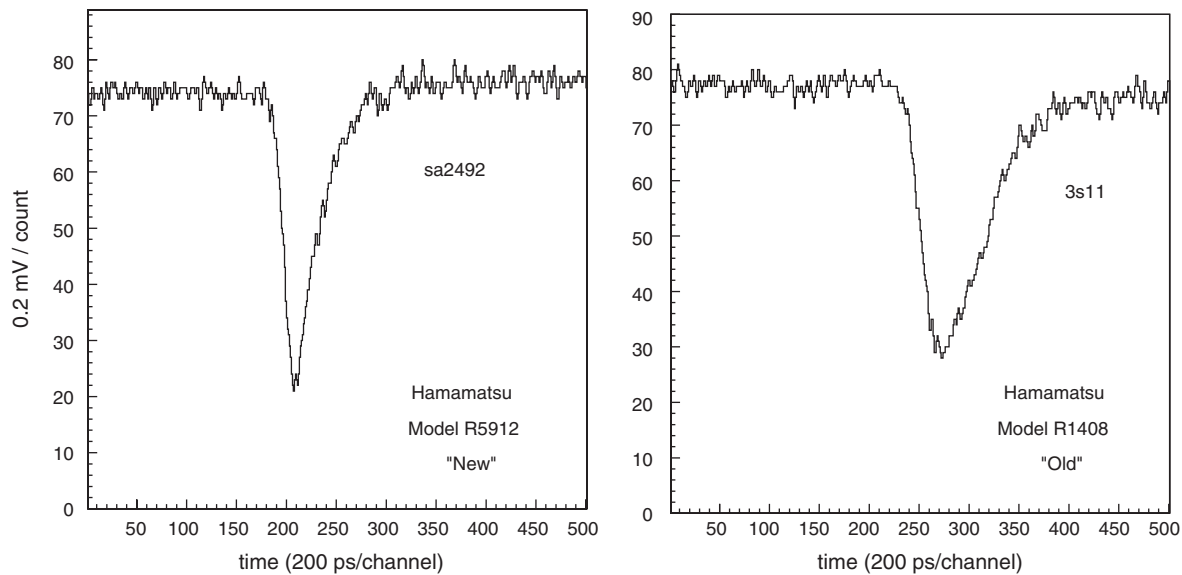


Fig. 6. Single photoelectron waveforms from the R5912 (left) and R1408 PMTs. Typical pulse widths were  $\sim 100$  channels or  $\sim 20$  ns. Each time window was 100 ns long.

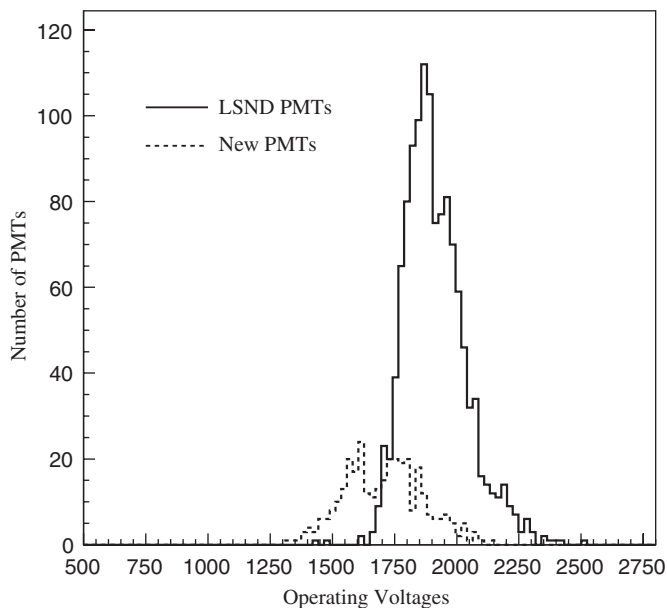


Fig. 7. Distribution of operating voltages for PMTs in the detector (from Ref. [6]).

parameters, especially the dependence of the PMT response on the angle of the incoming light. The data from R1408 and R5912 tubes were kept separate until the final analyses. The main objective of the angular tests was to find how the response of the PMTs depended on the angle of incident light. There were three additional tests. One tested a few tubes at various voltages. Another rotated the tubes about two orthogonal axes arbitrarily labelled “yaw” and “pitch” to test the assumption that the tubes are rotationally symmetric. The last tested tubes in air, without the oil present in the other tests.

#### 4.1. Angular tests: apparatus

The apparatus used for these tests is designed to replicate as closely as possible the characteristics of the MiniBooNE detector, on a much smaller and more manageable scale. The central part of the apparatus is a 40 gallon, stainless steel tank, painted on the inside with the paint used in the detector tank: a primer and black top coat. The primer is Hydralon P water-based epoxy primer (Sherwin Williams E72AC500/V66VC503 Hydralon P water-based epoxy primer), and the black topcoat is a flat black moisture cure aliphatic polyurethane chemical agent resistive coating (F93B102 Flat black moisture cure polyurethane). The tank can be filled with MiniBooNE oil when tests require it. It houses a single PMT, which can be rotated along the polar or azimuthal angle of the tube, using two precision rotary tables, one for pitch and one for yaw with respect to the table. The tubes were fixed to these tables with an arbitrary rotation, so “pitch” and “yaw” refer only to the mechanical apparatus and not any characteristic of the tubes. These tables have externally-coupled mechanical controls which allow the phototube position angle to be changed without opening the tank and exposing the tube to light. A 10.25 in. diameter window at the front of the tank allows the tests to simulate the light in MiniBooNE events by propagating the light several meters before it strikes the phototube. Because of this window, the entire testing room must be kept dark throughout each test.

The light source is a PicoQuant PLS 450, a sub-nanosecond pulsed LED. Its center wavelength is 460 nm, with  $50 \mu\text{W}$  average power at 40 MHz, approximately 30 nm spectral width, and typically 800 ps pulse width. It was used in 10 s sample periods at about  $10^6$  Hz. The light was filtered to produce a low-intensity beam ( $< 1$  photoelectron per pulse). The light was directed through an

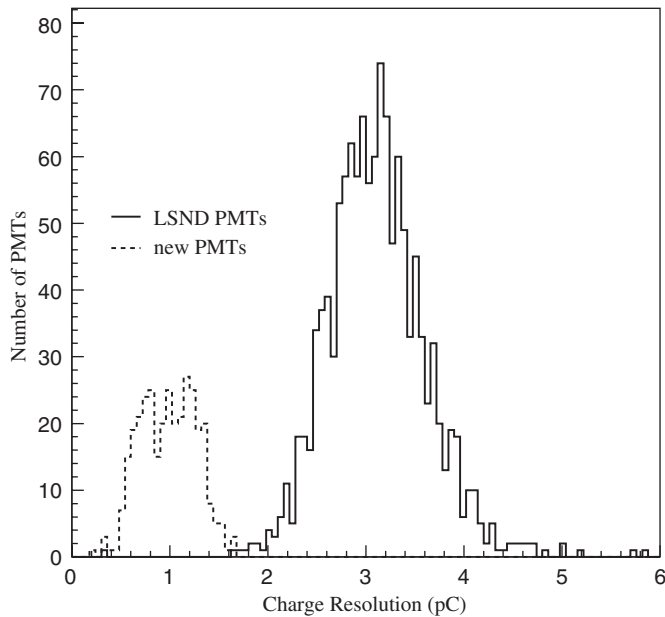


Fig. 8. Distribution of PMT charge resolutions (from Ref. [6]).

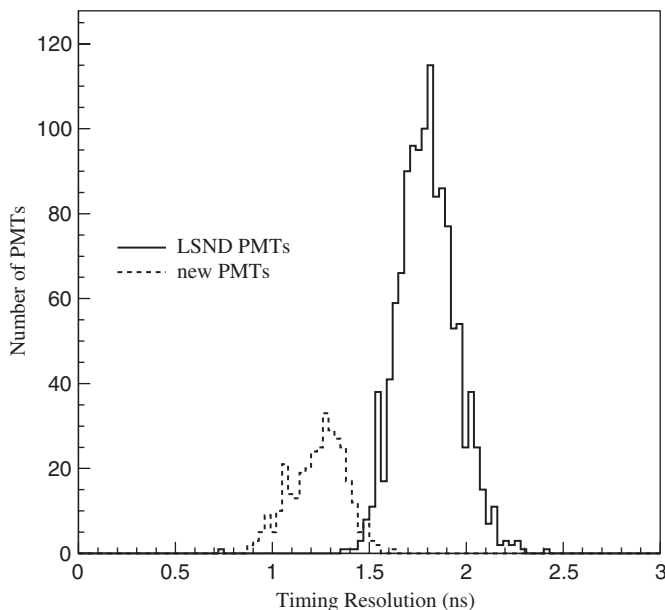


Fig. 9. Distribution of PMT time resolutions.

optical cable to face the tank from a distance of approximately 3 m. The light from this source makes a cone with half-angle about  $23^\circ$ , with greatest intensity along the centerline. The 3 m distance is great enough that one can assume that the entire face of the tube is uniformly illuminated with light in parallel rays.

The signals from the tube in the testing tank can be read out via an oscilloscope/GPIB card, or via the MiniBooNE data acquisition system. For the angular tests, a specialized data acquisition system was used (Fig. 11). The signal from the tube in the tank is amplified by a factor of 100, sent to a discriminator with 30 mV threshold, and finally put into coincidence with the delayed sync out signal from the LED

pulsar. The number of coincidences and the number of input light pulses each go to a scaler; they are then recorded and used to calculate the relative efficiency.

The tank is magnetically shielded with a  $\mu$ -metal box. This was done because ambient magnetic fields (e.g., the Earth's) can influence the relative efficiency of the tubes, and thus rotation within these fields may change the shape of the relative efficiency results. To see if ambient magnetic fields could have a significant effect, the tank was rotated (while holding the configuration of the tube and internal light source constant). The resulting effect was smaller than (but on the same order as) the angular dependence. When the tank was shielded and the same tests were performed, this dependence on orientation within ambient fields was not seen.

#### 4.2. Angular tests: procedures

The apparatus detailed above was used to study relative efficiency ( $E_{\text{rel}}$ ) as a function of angle. Using rapid, short-duration pulses of the LED, the  $E_{\text{rel}}$  of the tube was measured at a given position by taking the ratio of the number of responses which coincided with LED pulses to the total number of pulses, with about  $10^7$  pulses per datum.

$$\left( \frac{\text{coincidences out}}{\text{pulsar pulses in}} \right) = \text{relative efficiency } (E_{\text{rel}}).$$

$E_{\text{rel}}$  values were measured at  $5^\circ$  increments through the entire  $360^\circ$  of response, with two repetitions at each point and two rotations of the tube (from  $\theta = -180^\circ$  to  $\theta = +180^\circ$  and back again) for a total of four measurements at each tube position. Data were recorded directly into a spreadsheet, providing an ongoing real-time check.

This rotational test was performed on four R1408 and three R5912 tubes. Most of these tubes had been previously tested with the global testing (see Section 3), so the expected dark rate was known, and known to be comparable to that for the other tubes. The global testing results also specified tube operating voltages. It was necessary to dark adapt each tube for at least 12 h to obtain a dark rate comparable to that of the tubes in the detector, which have not been exposed to bright light for over 3 years.

The phototubes are essentially rotationally symmetric about their central vertical axis, with variation only in the dynode structure below the main dome. The R1408 tubes have “venetian blind” style dynodes; the R5912 tubes have “box and line” style dynodes. No significant differences were observed when the dynodes at the starting position were oriented horizontally, vertically, or at  $45^\circ$ . Additionally, a test was performed on one tube varying the yaw angle (similar to the pitch measurements performed on all tubes); again no significant differences were observed. The equivalence of pitch and yaw implies that the roll orientation of the tube does not affect the results. This simplified the measurements greatly.

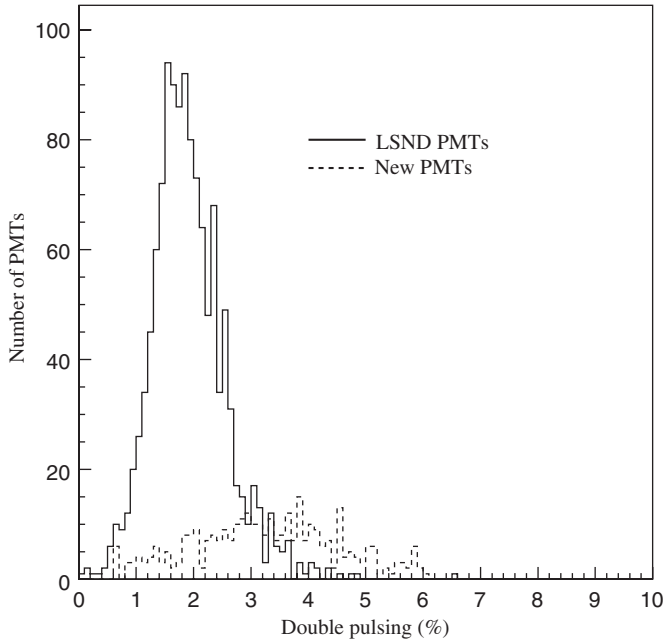


Fig. 10. Distribution of PMT double-pulsing rates.

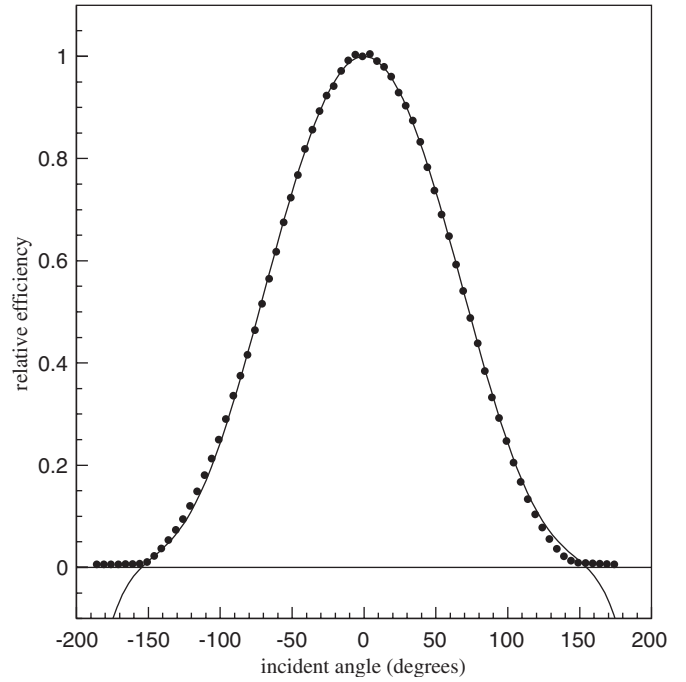


Fig. 12. A typical data set from an R1408 tube (19s3) with its symmetric polynomial fit. This fit uses the horizontal shift and maximum relative efficiency found from the initial quadratic fit.

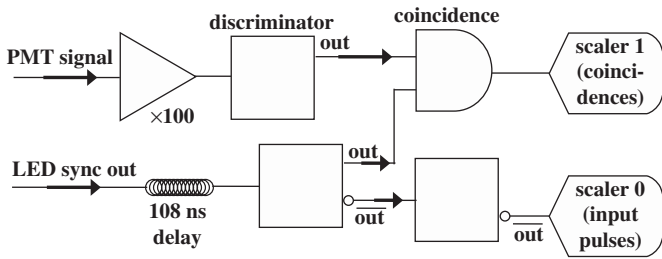


Fig. 11. Testing tank data acquisition system block diagram [7].

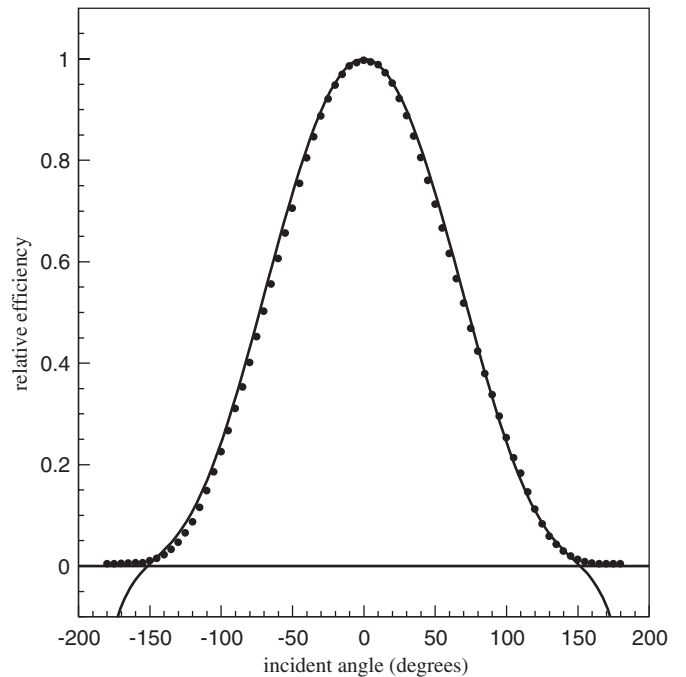


Fig. 13. A typical data set from an R5912 tube (SA2761) with its symmetric polynomial fit, analogous to Fig. 12.

Another test was performed by varying the operating voltages by 50 V above and below the nominal voltages found by previous MiniBooNE tests. The gain variation with voltage, which determines the max  $E_{rel}$ , was already known, so this test checked for variation in the shape of the  $E_{rel}$  curve more than the expected variations in amplitude. None of significance was observed.

### 4.3. Angular tests: results

Plots of relative efficiency as a function of angle were made for each set of measurements; these are roughly bell-shaped, as one would expect from the shape of the tubes. Typical results from an R1408 and an R5912 (with the fits as described below) are included in Figs. 12 and 13. These plots are similar from tube to tube (see Fig. 14). The parameters for the fits, as well as the average which will be used in the MiniBooNE Monte Carlo simulation, are included in Table 1. The results obtained were compared to expectations from the shape of the PMTs and results obtained by the SNO [8] experiment.

#### 4.3.1. Angular tests: results and polynomial fits

Because the PMT rotator mount inside the tank does not precisely specify the initial angle, max  $E_{rel}$  is found for each curve; the angle corresponding to max  $E_{rel}$  is assumed to



correspond to  $\theta = 0$ . Each plot's horizontal axis is shifted accordingly before the plots are compared. Each  $y$ -axis is scaled to  $\max E_{\text{rel}} = 1$ . An initial quadratic fit is performed on the central points of each plot to determine the horizontal shift. A six-degree polynomial fit is then performed on each plot in the region  $\theta = -150^\circ$  to  $\theta = 150^\circ$ . Outside of this region, statistics were significantly lower, making the data less comparable from tube to tube. The fit polynomial is forced to be symmetric by employing only even powers of the incident angle. The polynomial coefficients are varied to minimize the  $\chi^2$ . Finally, before comparing the functions, each fit is normalized by dividing by its constant term (which equals  $\max E_{\text{rel}}$ ), forcing

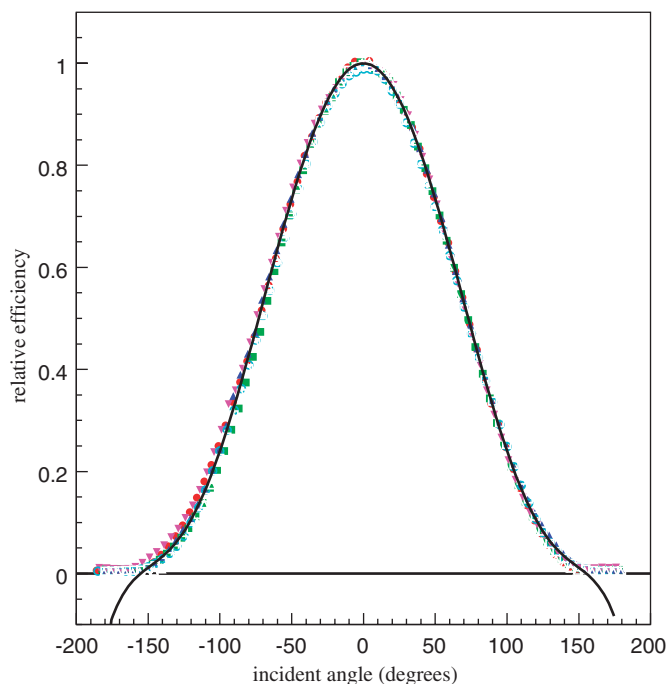


Fig. 14. Composite relative efficiency data. The data in each series were fitted to a polynomial, and normalized to  $\max E_{\text{rel}} = 1$  at  $\theta = 0^\circ$ . The average fit is shown.

Table 1  
Normalized parameters from all tubes tested

Tube number	$a_2$	$a_4$	$a_6$
15s3	$-1.182 \times 10^{-4}$	$5.018 \times 10^{-9}$	$-7.624 \times 10^{-14}$
19s3	$-1.234 \times 10^{-4}$	$5.436 \times 10^{-9}$	$-8.468 \times 10^{-14}$
20s1	$-1.162 \times 10^{-4}$	$4.818 \times 10^{-9}$	$-7.136 \times 10^{-14}$
20n16	$-1.156 \times 10^{-4}$	$4.725 \times 10^{-9}$	$-6.728 \times 10^{-14}$
SA2753	$-1.101 \times 10^{-4}$	$4.191 \times 10^{-9}$	$-5.539 \times 10^{-14}$
SA2761	$-1.177 \times 10^{-4}$	$4.964 \times 10^{-9}$	$-7.552 \times 10^{-14}$
SA2272	$-1.264 \times 10^{-4}$	$5.563 \times 10^{-9}$	$-8.549 \times 10^{-14}$
Average	$-1.182 \times 10^{-4}$	$4.959 \times 10^{-9}$	$-7.371 \times 10^{-14}$
Error	$5.337 \times 10^{-6}$	$4.583 \times 10^{-10}$	$1.042 \times 10^{-14}$
% Error	4.5	9.2	14.1

The error is the standard deviation from the average of the seven tubes tested. These parameters are to be used in the following function for the Monte Carlo simulation, where  $\theta$  is the angle of the incident light from the tube axis measured in degrees:  $E_{\text{rel}} = 1 + a_2\theta^2 + a_4\theta^4 + a_6\theta^6$ .

$\max E_{\text{rel}} = 1$ . The results of the fits are shown in Table 1 and superimposed on Figs. 14 and 18.

The errors on these data are dominated by tube-to-tube variation. The tests on each tube individually had very high statistics, typically around  $2 \times 10^7$  light pulses at each measured angle, and about 600 000 responses at central angles or 4000 at extreme angles (where the tube was facing backwards). Thus, to describe the error, it is more important to look at the relatively large differences between data sets from different tubes. This was done by examining the parameters of the fits. The average of the seven fitted values of each parameter and their standard deviation from that average are given in Table 1. Fig. 14 compares each PMT to the average fit, and deviations from the average fit are shown in Fig. 15.

The even-polynomial fits are sufficiently accurate and consistent for the R1408 tubes. For the R5912 tubes, the fits are less accurate on one side (see Fig. 13). To describe this difference, several other fits of the R5912 tube data were attempted. The main attempted non-symmetric fits used a different five-degree polynomial for angles above or below zero, requiring only that they meet at  $\theta = 0$ . The same horizontal shift and  $\max E_{\text{rel}}$  were used for this fit as for the initial, even polynomial fit. However, it was found that the variation between individual tubes was larger than the average difference between R5912 tubes and R1408 tubes, so the even polynomial fit was used for all tubes.

#### 4.4. Angular tests: comparison to predictions and to SNO data

MiniBooNE's relative efficiency angular data were compared to several geometrical models, and to data from previous tests from the Sudbury Neutrino Observatory (SNO) experiment [8]. The three geometrical models assumed the photocathode was a flat disk, a hemisphere, and the shape from the Hamamatsu technical specifications. The data from SNO were taken from tests on two R1408 PMTs in air and water, for a total of four tests. The PMTs in their detector are all Hamamatsu R1408 PMTs

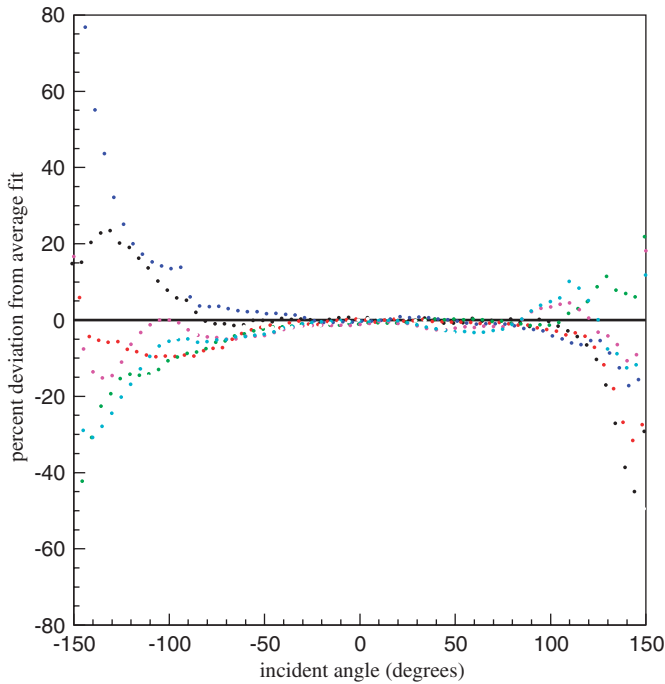


Fig. 15. Comparison of the data for each tube to the average fit. This plot shows, for each tube, the percent difference between the data and the average fit (i.e.,  $100 \times (E_{rel} - f(\theta))/f(\theta)$ ).

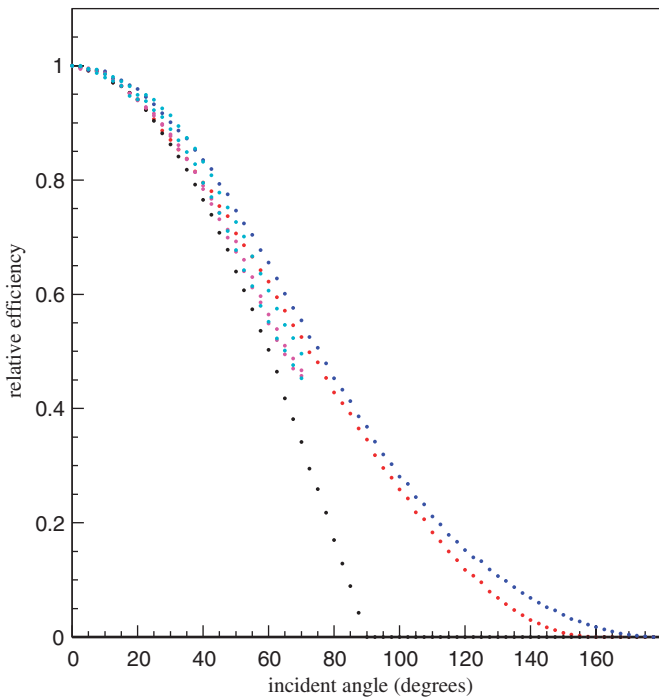


Fig. 16. Relative efficiency predicted by assuming that the PMT is a flat disk (black), a hemisphere (red), or ovoid shaped as in the Hamamatsu technical drawing (Fig. A.1) (blue), and the results found by SNO from testing two PMTs each in air (purple) and water (cyan).

(the same as the MiniBooNE R1408 tubes), making comparisons with them particularly useful. These seven results are shown together in Fig. 16. Note that all of the

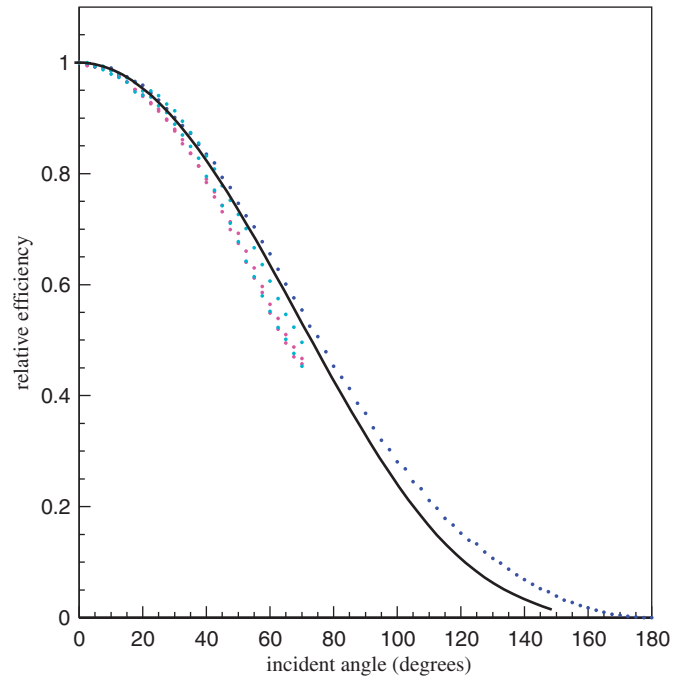


Fig. 17. Comparison of the average MiniBooNE  $E_{rel}$  function (black curve) with the SNO results from testing two PMTs each in air (purple) and water (cyan) and the geometrical  $E_{rel}$  function based on the Hamamatsu drawing (blue points).

SNO results lie between the hemisphere and the ovoid shape predictions on the top and the flat disk prediction on the bottom. SNO used water instead of oil because the SNO detector contains water (Fig. 17).

While developing the testing procedure, one tube was tested without filling the testing tank with oil. The results from this test, normalized to  $\max E_{rel} = 1$ , were very similar to the air tests done by SNO. This comparison is shown in Fig. 18.

Comparisons among the angular response measurements, SNO data, and geometrical models reveal overall similarities. The present data are also observed to be closer to the geometrical model from the Hamamatsu ovoid shape description than to the results obtained in either air or water by SNO. This may be the case because these data were taken in oil, where the index of refraction is much closer to that of glass than either air or water, resulting in less reflection at the oil–glass interface.

### 5. Implosion risk studies

On November 12, 2001, a PMT implosion in the Super Kamiokande (Super-K) [9,10] detector started a chain reaction that resulted in the loss of several thousand tubes. At the time, the MiniBooNE detector was not yet filled with oil. Assessment of the possibility of a similar accident occurring at MiniBooNE was immediately undertaken.

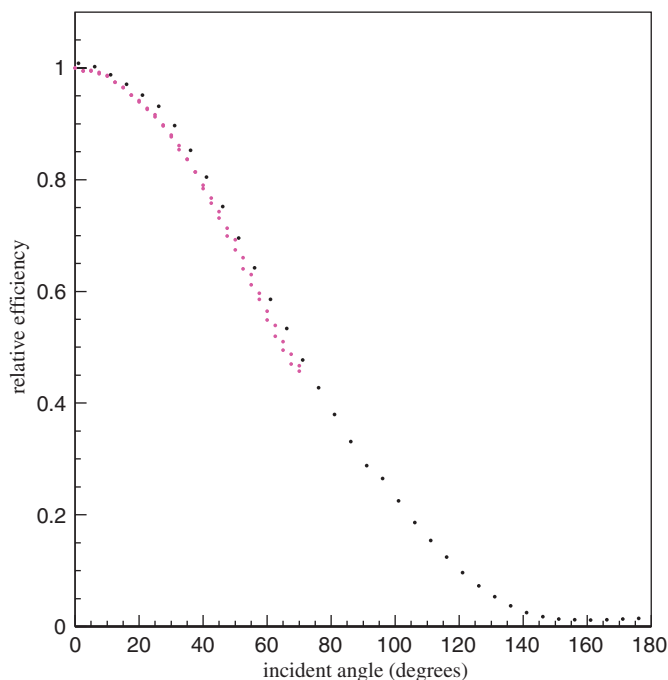


Fig. 18. Comparison of MiniBooNE data from the tube tested in air (black) to SNO test data taken in air (purple).

### 5.1. The Super-K detector design

The Super-Kamiokande detector is cylindrical, 36 m tall and 34 m in diameter, and filled with water. Hamamatsu 20-in. PMTs line the interior on a support structure. They are spaced 0.8 m center to center to give 40% photocathode coverage in the tank. These tubes are rated for a pressure of 608 kPa (6 atm). When full, the static pressure at the bottom of the detector is 208 kPa (2.05 atm).

At the time of the accident the tank was being refilled following some maintenance work, and was approximately  $\frac{2}{3}$  filled with water. The failure began with the implosion of a single tube on the detector floor; the reason for this failure is not known. This set off a chain reaction which ultimately destroyed most of the tubes more than 5 m below the water line. All tubes within 5 m of the surface survived.

### 5.2. Comparison of Super-K and MiniBooNE implosion scenarios

MiniBooNE has a significantly smaller (12 m diameter) spherical detector, using 8 in. Hamamatsu PMTs rated for 709 kPa (7 atm) pressure. The tubes are spaced 0.55 m center to center. The detector is filled with oil, which is a factor of 0.9 less dense than water. The static pressure at the bottom of the MiniBooNE tank is 208 kPa (4.5 atm). Each of these factors suggests that the MiniBooNE detector should be more resistant to a chain reaction of implosions than was the Super-K detector.

A computational model to calculate the shock wave pressure resulting from tube implosion was developed, based upon the stored energy in an evacuated tube at a given depth, assuming the pulse length is the tube radius. It should be noted that the energy stored in an 8 in. MiniBooNE tube is over an order of magnitude less than in a 20 in. Super-K tube.

The pressure on a neighboring tube when a tube at the bottom of the MiniBooNE detector implodes was compared to the pressure resulting from a Super-K implosion at a depth of 5 m, the depth above which all Super-K tubes survived. It was found the pressure in MiniBooNE was 0.45 times the Super-K pressure at survival depth, thus indicating a safety factor of two for MiniBooNE if the tubes were equally strong. In fact, the 8 in. tubes are rated for a higher pressure than the 20 in. tubes. MiniBooNE is therefore confident that the experiment is operating with a safety factor of greater than two, and that an accidental implosion of one of MiniBooNE's tubes will not result in a chain reaction.

A more rigorous hydrodynamic calculation was done using numerical techniques. From these calculations a somewhat greater safety factor of 2.6 can be inferred.

### 5.3. Tests performed at Super-K and SNO

After the Super-K accident, several tests were done at Super-K using the 20 in. tubes. Personal communication from several Super-K collaborators indicate that at a depth of 30 m of water chain reaction implosions occurred, but at 15 m there were no chain reactions. Since the pressure at 15 m is significantly greater than the maximum pressure in MiniBooNE this supports the conclusion that MiniBooNE tubes are not at risk for this sort of accident.

In 1990, the SNO collaboration also performed a series of tests of 8 in. PMTs in a water-filled pressure vessel. No chain reactions occurred at a pressure of 608 kPa (6 atm). This test also supports the previous conclusion.

## 6. Conclusion

This paper has reported on tests of the R1408 and R5912 photomultiplier tubes used in the MiniBooNE experiment. We have briefly described the global testing of all tubes, described in detail in Ref. [6]. The main results reported in this paper pertain to the phototube angular tests, and to the calculation of implosion risk for MiniBooNE. The angular response of the tubes determined a sixth order polynomial function describing the angular response. Implosion risk calculations for the tubes in the MiniBooNE detector were described. It was found that the MiniBooNE detector has a large safety factor.

### Acknowledgments

The authors would like to thank the following people for their valuable contributions: Jesse Guerra, Andy Lathrop,

Zhijing Tang, Ryan Patterson, T. Neil Thompson, Sally Koutsoliotas, and Christi Bohmbach. Thanks are also due to the following people for helpful discussions and editing: Bruce Brown, David Finley, Bill Louis, Peter Meyers, Mike Shaevitz, Ray Stefanski, and Morgan Wascko.

This material is based in part upon work supported by the National Science Foundation under Grants no. NSF PHY-0139464 and NSF PHY 00-98826 and the US Department of Energy no. DE-FG02-91ER40671.

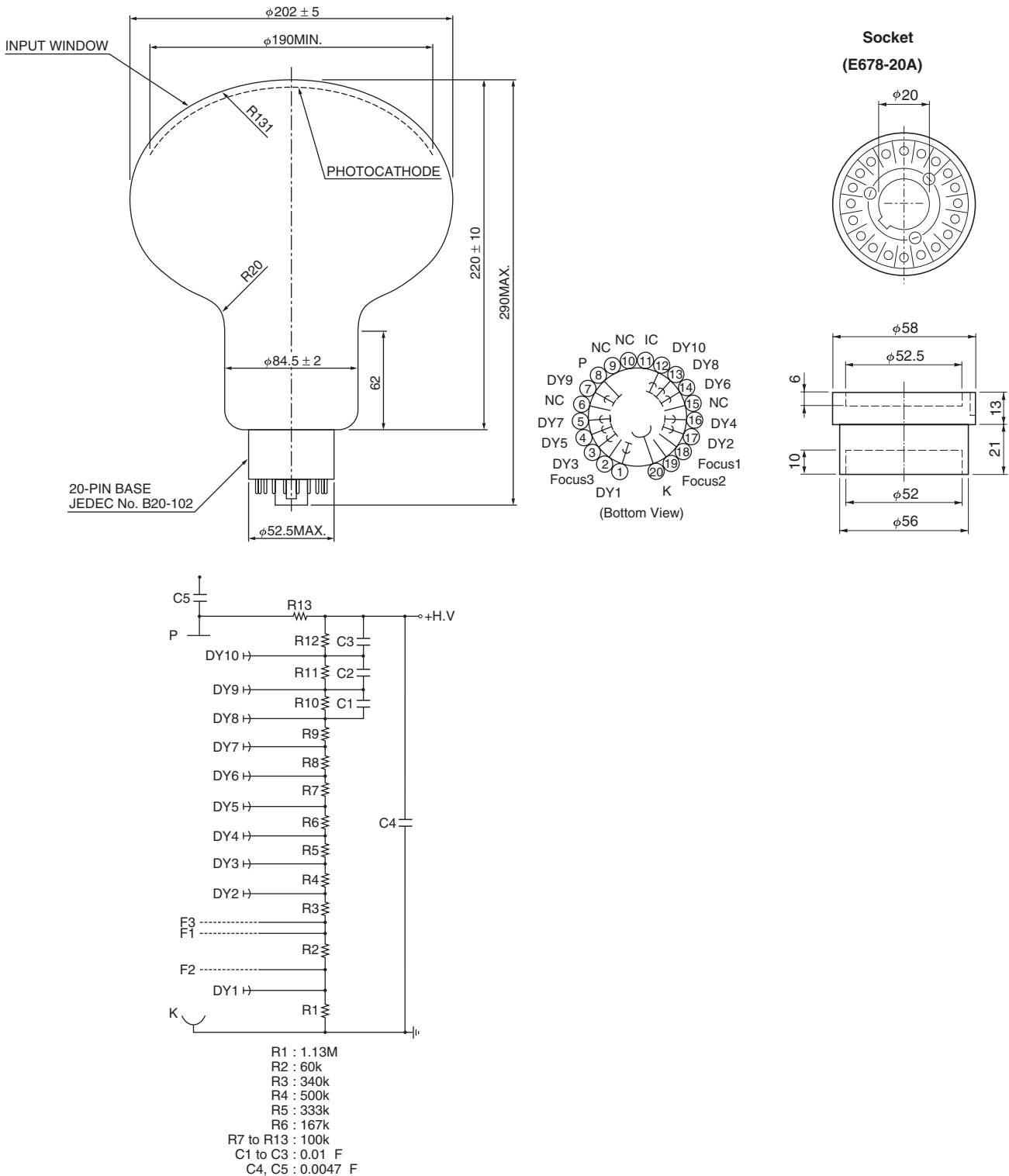


Fig. A.1. Technical design specifications for the R5912 phototubes from Hamamatsu [3]. Published with permission from Hamamatsu Photonics.

## Appendix A. Hamamatsu design specifications

Fig. A.1 shows the technical design specifications for the R5912 phototubes from Hamamatsu [3].

### References

- [1] Proposal for the MiniBooNE experiment: (<http://www.boone.fnal.gov/publicpages/proposal.ps>).
- [2] C. Athanassopoulos, et al., LSND Collaboration, Phys. Rev. Lett. 77 (1996) 3082 (arXiv:nucl-ex/9605003).
- [3] Hamamatsu Catalog, “Large Photocathode Area PMTs”, Catalog No. TPMH1286E02. (<http://usa.hamamatsu.com/>) (<http://www.hpk.co.jp/Eng/main.htm>).
- [4] MASTER BOND INC. 154 Hobart Street, Hackensack, NJ 07601, Web Site: (<http://www.masterbond.com>), phone: (201) 343-8983; fax: (201) 343-2132.
- [5] Loctite brand product, (<http://www.loctite.com>). In US Toll Free: 800-LOCTITE (800-562-8483). In Canada, call: 800-263-5043. Henkel Corp—Industrial, 1001 Trout Brook Crossing, Rocky Hill, CT 06067.
- [6] B.T. Fleming, L. Bugel, E. Hawker, V. Sandberg, S. Koutsoliotas, S. McKenney, D. Smith, IEEE Trans. Nucl. Sci. NS-49 (2002) 984.
- [7] J. May, M. Wysocki, L. Bugel, B.T. Fleming, P. Nienaber, D. Smith, Nuclear Science Symposium Conference Record, IEEE, vol. 1, 10–16 November 2002, pp. 446–449.
- [8] M.T. Lyon, Ph.D. Thesis, University of Oxford 59, 2002.
- [9] (<http://neutrino.phys.washington.edu/~superk>).
- [10] Fermi News, vol. 24(19), Fri Nov. 23, 2001.